Article

Neuron

Context-Dependent GluN2B-Selective Inhibitors of NMDA Receptor Function Are Neuroprotective with Minimal Side Effects

Highlights

- pH-dependent binding of a GluN2B modulator to the GluN1/GluN2B ATD heterodimer
- pH dependence renders a GluN2B modulator more potent at acidic pH during ischemia
- pH-dependent GluN2B inhibitors are neuroprotective in vivo with reduced side effects
- A novel dicarboxylate pH sensor establishes precedent for proton sensitive domains

Authors

Hongjie Yuan, Scott J. Myers, ..., James P. Snyder, Stephen F. Traynelis

Correspondence

strayne@emory.edu

In Brief

Yuan et al. describe a unique structure-activity relationship and the molecular mechanism governing pH sensitivity of GluN2B-selective NMDAR antagonists, which is clinically significant for neuroprotection during neuronal injury. They identify the dicarboxylate dimer as a new pH-sensitive motif within proteins.

Yuan et al., 2015, Neuron *85*, 1305–1318
March 18, 2015
http://dx.doi.org/10.1016/j.neuron.2015.02.008

CellPress

Neuron
Article

Context-Dependent GluN2B-Selective Inhibitors of NMDA Receptor Function Are Neuroprotective with Minimal Side Effects

Hongjie Yuan,[1,5] Scott J. Myers,[1,5] Gordon Wells,[2,5] Katherine L. Nicholson,[3,4] Sharon A. Swanger,[1] Polina Lyuboslavsky,[1] Yesim A. Tahirovic,[2] David S. Menaldino,[2] Thota Ganesh,[1] Lawrence J. Wilson,[2] Dennis C. Liotta,[2] James P. Snyder,[2] and Stephen F. Traynelis[1,*]
[1]Department of Pharmacology
[2]Department of Chemistry
Emory University, Atlanta, GA 30322, USA
[3]Department of Pharmacology and Toxicology
[4]Institute for Drug and Alcohol Studies
Virginia Commonwealth University, Richmond, VA 23298, USA
[5]Co-first author
*Correspondence: strayne@emory.edu
http://dx.doi.org/10.1016/j.neuron.2015.02.008

SUMMARY

Stroke remains a significant problem despite decades of work on neuroprotective strategies. NMDA receptor (NMDAR) antagonists are neuroprotective in preclinical models, but have been clinically unsuccessful, in part due to side effects. Here we describe a prototypical GluN2B-selective antagonist with an IC_{50} value that is 10-fold more potent at acidic pH 6.9 associated with ischemic tissue compared to pH 7.6, a value close to the pH in healthy brain tissue. This should maximize neuroprotection in ischemic tissue while minimizing on-target side effects associated with NMDAR blockade in noninjured brain regions. We have determined the mechanism underlying pH-dependent inhibition and demonstrate the utility of this approach in vivo. We also identify dicarboxylate dimers as a novel proton sensor in proteins. These results provide insight into the molecular basis of pH-dependent neuroprotective NMDAR block, which could be beneficial in a wide range of neurological insults associated with tissue acidification.

INTRODUCTION

The high mortality and morbidity of patients suffering from neurological damage as a result of cerebral ischemia, stroke, subarachnoid hemorrhage, or traumatic brain injury (TBI) constitute an enormous burden on society. Despite decades of research and multiple clinical strategies, there are few therapeutic alternatives for stroke apart from dissolution of the vessel clot in a subset of patients. A number of studies have shown that glutamate rises in injured tissue in animal models and human patients (see Table S1 available online). Virtually all neurons in the CNS express NMDA receptors (NMDARs), and without exception, overactivation of NMDARs is neurotoxic (Olney, 1969; Choi et al., 1988; Ellrén and Lehmann, 1989; Mody and MacDonald 1995; Wroge et al., 2012). Although numerous studies have confirmed the neuroprotective efficacy of NMDAR antagonists in animal models of injury (Table S2), multiple clinical trials with NMDAR antagonists failed to improve patient outcome in stroke or TBI (Table S3). Thus, a dichotomy exists between the lack of clinical efficacy and unequivocal preclinical data showing that NMDAR blockade within hours of ischemia reduces neuronal death in multiple species (Table S2). Post hoc analyses of clinical trials involving NMDAR antagonists have identified several factors that may account for their failures (Morris et al., 1999; Albers et al., 2001; Sacco et al., 2001; Gladstone et al., 2002; Farin and Marshall 2004). The most commonly discussed shortcomings include (1) the presence of dose-limiting side effects that prompted reduced therapeutic exposures, (2) the administration of NMDAR antagonists after an effective temporal window (several hours postinjury) recognized in animal studies, (3) the heterogeneity of ischemic injuries, and (4) the lack of quantifiable clinical endpoints. The latter could be addressed with careful management of the clinical trial, inclusion criteria, and postinjury analysis (Kidwell et al., 2001; Narayan et al., 2002). Advances in clinical trial design have dramatically shortened the time to administer neuroprotectants to patients (Saver, 2013), bringing delivery in line with therapeutic windows for efficacy demonstrated in preclinical studies. If clinical treatments can be delivered within 2 hr by first responders, NMDAR antagonists with expanded tolerability margins could become useful therapeutic agents. To improve the tolerability profile of NMDAR antagonists, we sought to limit GluN2B receptor antagonism to the affected regions and times at which brain injury occurs, thereby reducing overall side effects.

It has long been known that ischemia is associated with tissue acidification as a result of altered energy production and failure to clear tissue CO_2 (Kaplan et al., 1987; Matsumoto et al., 1990; Katsura et al., 1992). Tissue acidification can reach pH 6.9 in penumbral regions that are protected by NMDAR antagonists in animal models of ischemia, and pH 6.5 in the ischemic core (Mutch and Hansen 1984; Smith et al., 1986; Nedergaard

Table 1. Optimization of pH Dependence of GluN1/GluN2B Antagonists as a Function of N-Alkyl Chain Length and Steric Bulk

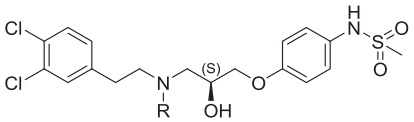

R[a]	#	Chain Amine pKa[b]	Fold Increase in Ionized Species[c]	N-Substituent Volume Angstroms^3	IC_{50} pH 6.9 μM (N) [d]	IC_{50} pH 7.6 μM (N) [d]	IC_{50}(7.6)/IC_{50} (6.9) Ratio [e]
-H	(*S*) 93-4	8.6	1.1	–	0.036 (10)	0.045 (11)	1.3
$-CH_3$	(*S*) 93-2	8.0	1.3	19.8	0.050 (29)	0.13 (22)	2.6
$-CH_2CH_3$	(*S*) 93-5	8.1	1.2	33.4	0.021 (22)	0.067 (14)	3.2
$-CH_2CH_2CH_3$	(*S*) 93-6	8.1	1.2	47.9	0.094 (17)	0.48 (16)	5.1
$-CH_2CH_2CH_2CH_3$	(*S*) 93-31	8.1	1.2	62.3	0.19 (32)	1.8 (23)	9.4
$-CH_2CH_2CH_2CH_2CH_3$	(*S*) 93-87	8.1	1.2	77.5	0.16 (9)	0.60 (6)	3.8
$-CH(CH_3)_2$	(*S*) 93-115	8.2	1.2	47.9	0.19 (11)	0.62 (12)	3.3
$-CH_2CH(CH_3)_2$	(*S*) 93-97	8.0	1.3	63.6	1.1 (21)	3.2 (31)	2.9

See also Figure S1 and Table S6.

[a]Compound synthesis described in Tahirovic et al. (2008); all compounds were the *S*-enantiomer.

[b]The pKa of the chain nitrogen was calculated using ACD/pKa DB 12.00 (http://www.acdlabs.com).

[c]Fold increase ionized species when reducing pH from 7.6 (pH1) to 6.9 (pH2) was calculated using Equation 3: the Henderson-Hasselbach equation as

$$\left(1+10^{(pH2-pKa)}\right)/\left(1+10^{(pH1-pKa)}\right). \quad \text{(Equation 3)}$$

[d]IC_{50} values for inhibition of GluN1/GluN2B expressed in *Xenopus* oocytes were determined as described in the Experimental Procedures from composite inhibition curves. N is the number of oocytes recorded; measurements were made for oocytes at both pH values in the same experiment. The slope varied from 0.70 to 1.09; maximum inhibition 79%–100%.

[e]The pH-dependent potency ratio for inhibition of GluN1/GluN2B receptors.

et al., 1991; Katsura and Siesjo, 1998). We studied pH dependence of GluN2B-selective NMDAR antagonists (Pahk and Williams 1997; Mott et al., 1998; Wang et al., 2014) using medicinal chemistry to synthesize compounds that were maximally potent and effective in ischemic tissue, yet minimally potent in healthy brain. Our goal was to identify a novel class of clinically relevant NMDAR antagonists with expanded tolerability/safety margins compared to previous generations of NMDAR antagonists. Here we describe the mechanistic and structural basis for pH-sensitive GluN2B-selective antagonists and demonstrate their utility as neuroprotectants in vivo.

RESULTS

pH-Sensitive GluN2B-Selective Antagonists

We evaluated the pH sensitivity of multiple GluN2B-selective noncompetitive antagonists identified by bioinformatic criteria as diaryl compounds with a nitrogen-containing linker and >10 Å separation between terminal aromatic rings (Chenard and Menniti 1999). Among these, the *S*-enantiomeric analogs of the propanolamine AM-92016 (93-2, Table 1) emerged as a potent, synthetically tractable class of molecules that showed systematic variations in pH sensitivity. We subsequently evaluated the pH dependence of over 200 analogs on rat GluN1-1a/GluN2B receptors (hereafter GluN1/GluN2B) expressed in *Xenopus laevis* oocytes (Tahirovic et al., 2008; Mosley et al., 2009), including the series of N-alkyl-substituted analogs summarized in Table 1. Within this subseries, an optimal length of the N-alkyl chain, compound 93-31 (four carbons), maximized the pH sensitivity and showed an order of magnitude shift in potency per half-log unit change in pH in *Xenopus* oocytes (Table 1). Figures 1A and 1B show similar effects of pH on concentration-effect data for 93-31 inhibition of GluN1/GluN2B receptors expressed in HEK293 cells recorded under voltage clamp. Although inhibition observed in mammalian cells is more potent (pH 6.9, IC_{50} = 0.040 μM) compared to *Xenopus* oocytes, the potency is enhanced 9.0-fold at acidic pH. We subsequently tested the effects of 93-31 on triheteromeric NMDARs that contain one copy each of GluN2A and GluN2B (Hansen et al., 2014). Although triheteromeric receptors show reduced sensitivity to GluN2B-selective inhibitors (Hatton and Paoletti 2005; Hansen et al., 2014), compound 93-31 still showed 4.4-fold enhanced potency at acidic pH at GluN1/GluN2A/GluN2B receptors (Figure S1), suggesting it will retain pH sensitivity at triheteromeric receptors expressed in adult cortex. We selected compound 93-31 as a prototype to evaluate the mechanism of pH-sensitive NMDAR inhibition.

Mechanism Underlying pH Sensitivity of GluN2B Antagonists

One potential explanation for the pH sensitivity of 93-31 could be a systematic change in the pKa of the tertiary amine in the diaryl linker that could alter the fractions of ionized and unionized ligand, and thus alter potency. This occurs with phosphono-containing competitive antagonists, leading to lower concentrations of the more active species, which reduces potencies for these competitive antagonists under acidic conditions (Benveniste and Mayer 1992). Table 1 summarizes the predicted free solution pKa values of the tertiary amine in this series, and shows that the relative abundance of ionized or unionized species does not account for pH-dependent potency. In addition, we also examined

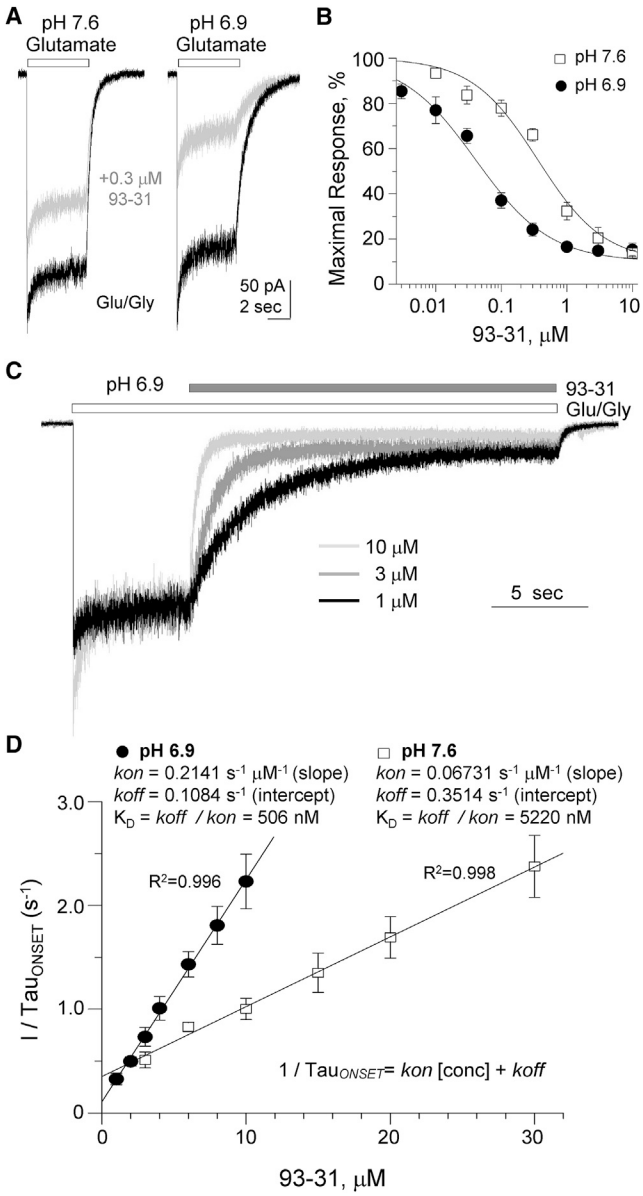

Figure 1. Proton-Sensitive Inhibition of GluN1/GluN2B NMDARs

(A) Representative whole-cell current recordings from HEK cells transiently expressing rat GluN1/GluN2B receptors. Current responses were elicited by 100 μM glutamate (open bar) in the absence of (black) or presence of 0.3 μM 93-31 (gray) at pH 7.6 (left panel) and pH 6.9 (right panel) (V_{HOLD} = −60 mV). Glycine (30 μM) was present in all the recording solutions.

(B) Composite concentration-response curves at pH 7.6 and pH 6.9 for compound 93-31 determined by whole-cell currents recorded from HEK cells transiently expressing GluN1/GluN2B receptors.

(C) Representative whole-cell currents recorded from HEK cells transiently expressing rat GluN1/GluN2B receptors were elicited by 100 μM glutamate and 30 μM glycine (open bar), followed by coapplication of glutamate and glycine plus increasing concentrations of 93-31 (filled bar) at pH 6.9 (V_{HOLD} = −60 mV).

(D) Plot of the reciprocal of the fitted time constant describing the onset of inhibition as a function of 93-31 concentration at pH 6.9 (filled circles) and pH 7.6 (open squares) is shown with fitted linear regression superimposed. Insets display the calculated *kon*, *koff*, and K_D values at each pH. All data are presented as mean ± SEM. See also Figure S1 and Table S4.

the branched chain analogs *iso*-propyl (93-115) and *iso*-butyl (93-97), which show less pH sensitivity (Table 1). For example, compound 93-97, the *iso*-butyl isomer of 93-31, showed a similar pKa but only a 2.9-fold increase in potency at lower pH values, compared to a 9.4-fold increase for the straight chain isomer 93-31. These data exclude the possibility that pH-induced changes in ligand ionization account for the proton sensitivity for inhibition of GluN1/GluN2B receptors.

To investigate the mechanism underlying proton sensitivity, we evaluated whether extracellular pH alters the rates at which 93-31 binds to and dissociates from the receptor. We expressed GluN1/GluN2B receptors in HEK cells and performed rapid agonist/modulator concentration jumps while recording the whole-cell current. The onset of inhibition following application of compound 93-31 (Figure 1C) could be well described by a single exponential function, allowing us to determine the association and dissociation rate constants for 93-31 at two different pH values by analyzing the concentration dependence for onset of inhibition (Figure 1D).

Analysis of these data suggests that increasing the proton concentration slowed the dissociation rate k_{OFF} and increased the association rate k_{ON} (Figure 1D; Table S4). This decreased the K_D by 10.3-fold at pH 6.9 compared to pH 7.6. We interpret these data to suggest that the pH sensitivity of the association and dissociation rates (and thus binding) for compound 93-31 accounts for the proton sensitivity of the IC_{50} (Table S4). Given the minimal effect of pH on ligand ionization (Table 1), agonist EC_{50} (Traynelis et al., 1995), and response time course (Banke et al., 2005), we hypothesized that the proton-sensitive inhibition reflects altered protein conformation, or an altered set of side-chain rotamers and/or ionization states at acidic pH that renders compound 93-31 a more potent inhibitor.

Binding of pH-Sensitive Antagonists

To explore the structural basis for the pH sensitivity of the 93-series compounds, we docked the compounds in Table 1 into a model derived from crystallographic data for a structure of *Xenopus* GluN1-ATD dimerized with rat GluN2B-ATD (3QEL, Karakas et al., 2011). Figure 2 shows a high scoring pose of 93-31 docked into the ifenprodil binding site (Figures 2A–2D). From these docking studies it is clear that 93-31 can adopt a pose similar to that determined for ifenprodil with molecular contacts analogous to those described for other propanolamines (Burger et al., 2012). For example, the chlorophenyl ring of 93-31 overlays the phenyl ring of ifenprodil in a hydrophobic pocket defined by GluN1-Tyr109 and GluN2B-Phe114/Ile82 (Figures 2C and 2D), while the phenylether moiety of 93-31 is superimposed on the phenol ring of ifenprodil and the sulfonamide matches the phenol hydroxyl group (Figure 2E). The tertiary amine of 93-31 occupies the same region as its ifenprodil piperidine counterpart (Figures 2B and 2E). When docking with the central tertiary nitrogen protonated (*S*-enantiomer), the ammonium group is predicted to make favorable contact with GluN2B-Gln110 (Figure 2C), which is also simultaneously able to interact with the ether moiety of 93-31. The hydroxyl group is able to form a hydrogen bond with the side-chain carboxyl of GluN2B-Glu106. All ligands shown in Table 1 docked in a similar fashion.

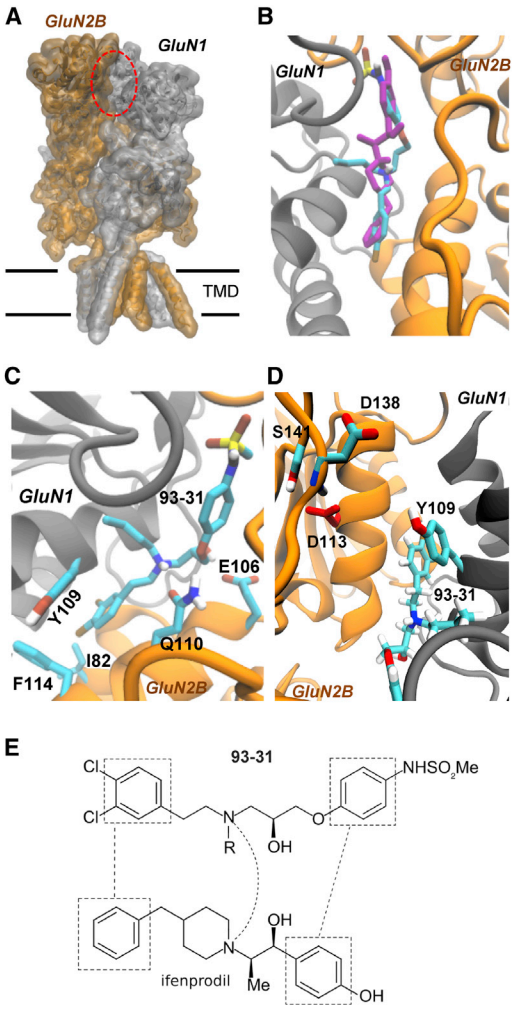

Figure 2. Binding of 93-31 to the GluN1/GluN2B ATD Heterodimers

(A) A model of the GluN1/GluN2B NMDAR built from crystallographic data for the NMDAR (Karakas and Furukawa, 2014). The red ellipse indicates the ifenprodil binding site within the amino-terminal domain at the interface of GluN1 and GluN2B.

(B) Superimposed conformations of 93-31 (cyan) and ifenprodil (magenta) docked into the ATD dimer (Karakas et al., 2011; see Experimental Procedures).

(C) The bichlorophenyl ring sits in a hydrophobic pocket defined by GluN1-Tyr109 and GluN2B-Ile82/Phe114. The amino group is predicted to interact with GluN2B-Gln110, and Glu106 hydrogen bonds with the hydroxyl moiety.

(D) Reversed view of 93-31 showing interactions with GluN1-Tyr109, and GluN2B-Asp113, which is predicted to have an elevated pKa within the protein compared to free solution.

(E) Juxtaposed functional groups of ifenprodil (3QEL) and 93-31 (from left to right, chlorophenyl/phenyl, tertiary amine, and sulfonamide/phenol); R is *n*-butyl.

Examination of the binding pockets represented in structures for ifenprodil and Ro 25-6981-bound ATD heterodimer (3QEL and 3QEM) reveals a small 8 Å tunnel leading away from the binding site interface toward the GluN1 subunit that is lined primarily by hydrophobic side chains (Figures 2B and 3A). This passageway is close to the chain nitrogen of the N-substituted propanolamines, raising the possibility that it might be involved in the differential properties observed for the different-sized alkyl substituents on this nitrogen. Extensive induced-fit docking suggested that the N-alkyl derivatives can occupy and exploit the space created by this tunnel (Figure 3A). We therefore tested whether inhibition of receptors by 93-series compounds is altered by mutations at residues forming this tunnel, choosing side chains for substitutions that occlude the tunnel but do not otherwise perturb the overall protein structure (confirmed by molecular dynamics simulations, Figure S2), such as GluN1(G112A). Modeling places the alanine side-chain methyl within the tunnel, effectively occluding it. If the existence of this tunnel provides additional space for N-alkyl derivatives, then occlusion should alter IC_{50} for *n*-butyl-substituted 93-31, but not that of the unsubstituted analog 93-4 (Figures 3B and 3C). Concentration-effect curves for these two inhibitors against wild-type GluN1/GluN2B and GluN1(G112A)/GluN2B mutant receptors in oocytes showed that the IC_{50} for 93-31 was increased 6-fold at pH 6.9 from 0.19 to1.2 μM (n = 23–29 oocytes) without a change in slope (0.8–0.9) or fitted minimum (17%–20%), consistent with the idea that this tunnel altered the binding of this ligand. Further, the pH sensitivity of 93-31 was reduced to 3.8-fold by the GluN1(G112A) mutation (Figure 3D; Table 2). By contrast, 93-4 which lacks an N-linked substitution showed only a 2-fold increase in the IC_{50} from 0.036 μM at wild-type GluN1/GluN2B (n = 10) compared to 0.070 μM at GluN1(G112A)/GluN2B (n = 8) mutant receptors with no change of pH sensitivity (1.4-fold) for inhibition (Figure 3E). These results were not a reflection of a change in the receptor's inherent pH sensitivity, as the ratio of maximum receptor current at pH 6.9 to 7.6 for GluN1(G112A)/GluN2B (0.21 ± 0.01, n = 8) was identical to that for wild-type GluN1/GluN2B (0.21 ± 0.01, n = 8, p = 0.92). These data are consistent with the idea that ligands with N-alkyl substitutions can take advantage of space afforded by this tunnel.

Identification of pH-Sensitive Binding-Site Residues

We next explored whether ionizable residues near the binding site might be involved in the pH-dependent change in association rate for 93-31. The pKa values for 20 ionizable residues in the GluN1/GluN2B dimer (3QEL) within 12 Å of the ifenprodil binding pocket were calculated (Figure 4A; Table 2). Predicted pKa values (pKa*) for ionizable side chains caused by the surrounding microenvironment suggest that some residues may experience a locally induced pKa shift, rendering side-chain ionization(s) sensitive to a decrease in pH to 6.9, as occurs in the ischemic penumbra (Table 2). Among the 20 residues, several pKa* values were predicted to be substantially elevated relative to their free solution values, including a pair of closely spaced acidic residues (Figures 4A and 4B), GluN2B-Glu106 (N terminus of helix-3, pKa* 7.0) and GluN2B-Glu235 (C terminus of helix-8, pKa* 5.1). The side-chain rotamer of Glu235 in a crystal structure solved at pH 7.5 (3QEL) is oriented away from Glu106 (Figure 4B), and thus the latter only contributes a small increase to the predicted pKa of Glu235 (ΔpKa* 0.8). GluN2B-Glu106 is less solvent exposed than Glu235, and thus is more likely to have an elevated pKa*. At pH 6.9, about half of the Glu106 residues (pKa* 7.0) at any moment will be protonated. Protonation of either of these residues is predicted to

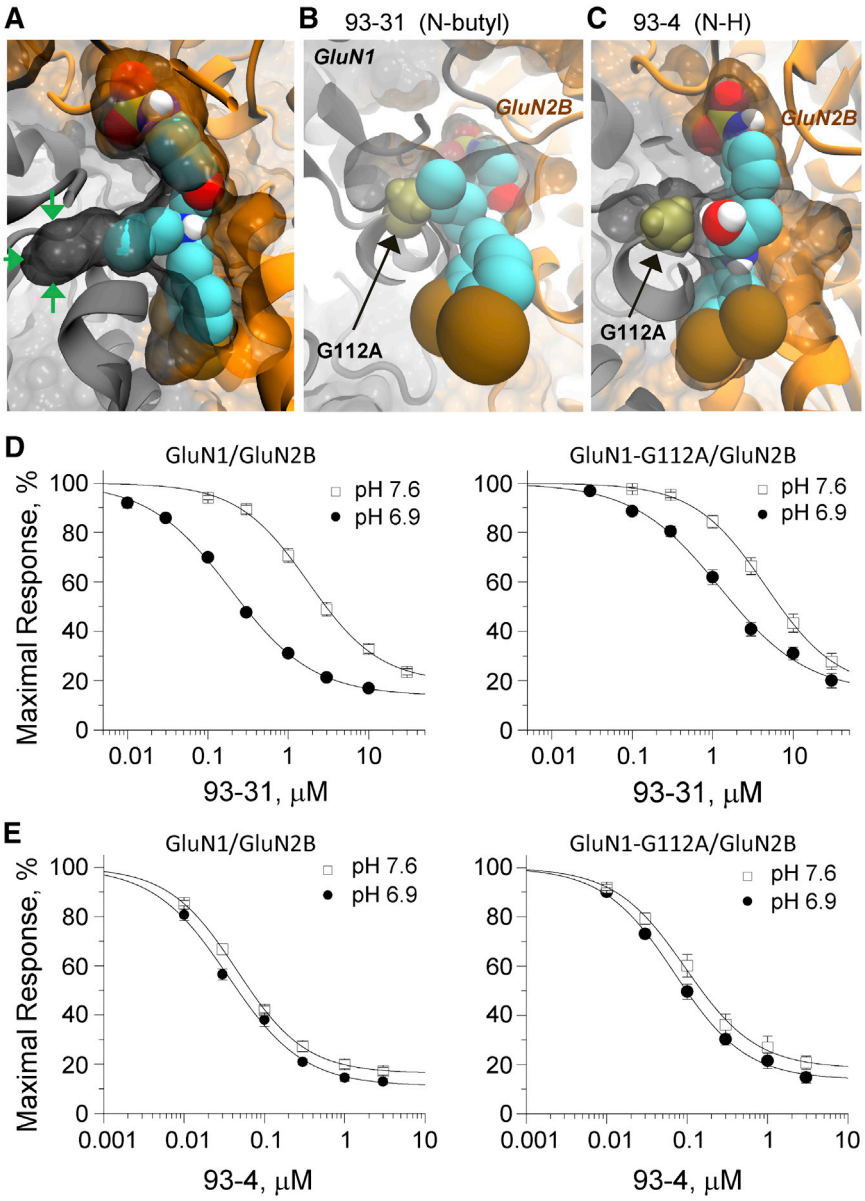

Figure 3. Exploitation of a GluN1 Tunnel at the ATD Heterodimer Interface by 93-31

(A) Spacefill illustration of the tunnel entering into GluN1 (green arrows) with an induced-fit docked pose of 93-31 showing that the *n*-butyl substituent on the chain nitrogen protrudes into and fills this space.

(B) Occlusion of the GluN1 tunnel by the mutation GluN1(G112A), shown as a bronze spacefill, clashes with the *n*-butyl group of 93-31 in this docked pose.

(C) The GluN1(G112A) mutation, shown as a bronze spacefill, does not interact with docked pose of 93-4, which lacks any substituent on the chain nitrogen. The bichlorophenyl ring is at bottom.

(D and E) Concentration effect curves for 93-31 (D) or 93-4 (E) inhibition of GluN1/GluN2B (left panel) and GluN1(G112A)/GluN2B (right panel) responses in oocytes. All data presented as mean ± SEM. See text for fitted IC_{50} values. See also Figure S2.

allow a favorable interaction, enhanced by the formation of a carboxylic acid dimer, if both are protonated. This hypothesis is partially confirmed by a second crystal structure of GluN2B at pH 5.5, in which presumably protonated Glu235 interacts directly with Glu106 as a dimer (3JPW; Figure 4B). The local conformational reorganization is in striking contrast to structural data obtained at pH 7.5, which shows the side chain directed toward bulk solvent (3QEL). This difference in Glu235 orientation between the two structures was not previously noted (Karakas et al., 2009, 2011). We suggest that at lower pH, protonation of Glu106 and/or Glu235 is favored, allowing for these residues to interact noncovalently. Glu235 and Glu106 reside at the N termini of two helices, and ifenprodil (and presumably 93-31) inhibits GluN1/GluN2B by restricting domain movement. Thus, if Glu106 and Glu235 interact more strongly at lower pH, this could add a further restriction to intradomain movement in addition to ligand binding. Rigid rotation of Glu235 within this structure (3QEL) so that it forms a bidentate interaction with Glu106 shifts the predicted pKa* values still further away from the free solution values to 6.8 (Glu235) and 7.9 (Glu106). To explore the effects of the dicarboxylate on the ligand, charge-neutral subsets of all nearby residues were used to generate electrostatic potential surfaces (see Experimental Procedures). While there was no noticeable change on the predicted partial charges of 93-31, the electrostatic surface potential charge centered on the ammonium group of 93-31 was more positive in the presence of the Glu106:Glu235 carboxylic acid dimer (Figure 4C). Based on the structural differences in Glu106 and Glu235 for crystals solved at different pH values (3JPW versus 3QEL), and the predicted pKa* values, the amino acid pair Glu106:Glu235 is a strong candidate for constituting a pH sensor that influences 93-31 binding and inhibition.

Carboxylic Acid Dimers: An Unrecognized Interaction within Proteins

The interaction between Glu106 and Glu235 at pH 5.5 in 3JPW is somewhat unusual and suggestive of a hydrogen bonded carboxylic acid dimer (Figures 4B and 4C). This bidendate dimeric form is well-represented in small-molecule crystallography, with the Cambridge crystallographic database (Allen 2002) reporting ~2,000 cases when queried with Mercury/Motif (Leiserowitz et al., 2002; Macrae et al., 2006). In addition, in the appropriate solvent and gas phase, carboxylic

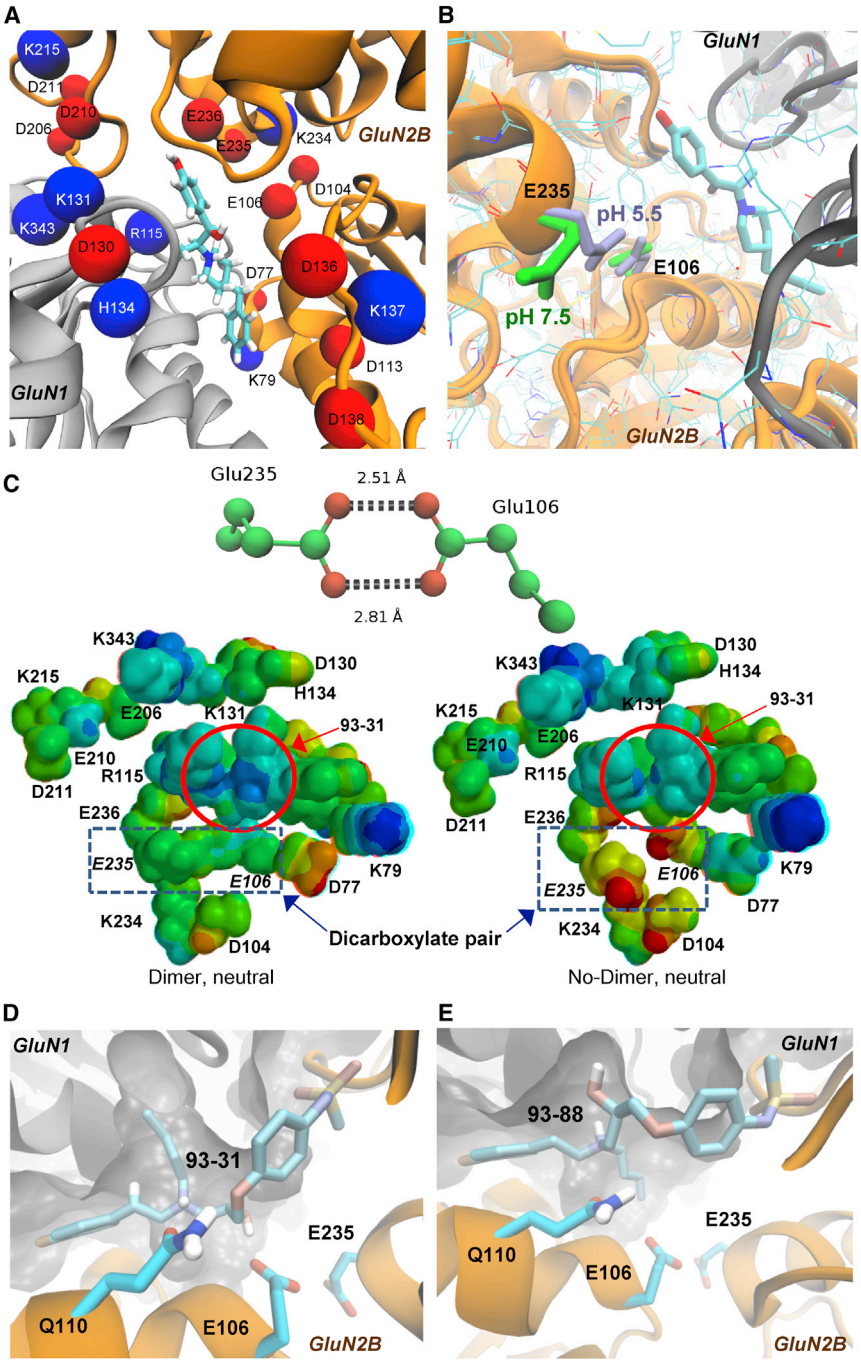

Figure 4. Mutation of Candidate Residues for Controlling the pH Sensitivity of 93-31 Binding

(A) Acidic (red) and basic residues (blue) are shown within 12 Å of the ifenprodil (depicted as cyan sticks) binding site. We estimated the intraprotein pKa values using PropKa 3.1 (see Experimental Procedures and Table 2), and subsequently mutated these residues to Ala to determine their effect on the pH sensitivity of the IC_{50} for 93-31. GluN1 is shown as gray, and GluN2B is orange.

(B) Glu106 and Glu235 are close enough to interact at the lower pH of 5.5 (light blue, 3JPW), but not at pH 7.5 (green, 3QEL) in GluN2B crystal structures.

(C) (Top panel) Distances in Å are shown separating Glu235 and Glu106 in the crystal structure for GluN2B solved at pH 5.5 (PDB code 3JPW), implying O-protonation and O-H hydrogen bonds of ~1.6 Å and 1.9 Å, respectively. (Bottom panel) Electrostatic potential surfaces on a truncated 93-31 binding site (in red circle) were predicted with Spartan using the PM6 basis set. 93-31 is more positive (blue) in the presence of the carboxylic acid dimer between E106 and E235 (left) compared to the noninteracting charged state (right). Both PM6 models are charge neutral, each containing an equal number of cationic and anionic side chains surrounding the binding site.

(D) Occupation of the tunnel by *n*-butyl of 93-31 potentially orients the hydroxyl for interaction with Glu106.

(E) A similarly scoring docking pose of the *R*-enantiomer of 93-31 (93-88) orientates the hydroxyl away from Glu106 and toward the tunnel. See also Figure S3.

dimers are readily formed (Tzeli et al., 2011; Shipman et al., 2007). However, scanning the PDB for residues with the dimer geometry revealed 41 structures exhibiting a similar interaction between carboxylate side chains, none of which were discussed, with the exception of a carboxylic acid dimer between retinoic acid and Glu121 in a quintuple mutant of the cellular retinoic acid binding protein (3CWK; Vasileiou et al., 2009). The present results suggest that carboxylic acid dimers may represent a hitherto-unrecognized functional interaction in proteins.

Potential Role of Glu106:Glu235 in pH-Sensitive 93-31 Inhibition

Inspection of 93-31 docking poses in the GluN1/GluN2B ATD heterodimer at pH 7.5 suggests several possible roles for GluN2B-Glu106 and -Glu235 in terms of conferring pH sensitivity. The top scoring docking results suggest that Glu106 can hydrogen bond with 93-31, while Glu235 is close enough to interact electrostatically with the ligand (Figures 4B and 4C). Occupation of the tunnel by *n*-butyl orients the hydroxyl for a favorable interaction with Glu106, the orientation of which we propose is pH sensitive (Figure 4D). Interestingly, docking of the *R*-isomer of 93-31 (93-88; Figure 4E) places the *n*-butyl chain outside of the tunnel and orients the hydroxyl group away from Glu106 in similarly high-scoring poses. This docking result is consistent with the significantly reduced pH sensitivity of 93-88 inhibition (3.8 ± 0.7-fold shift in IC_{50} at pH 6.9 compared to the IC_{50} at pH 7.6) versus 93-31 (10 ± 2.7-fold shift, n = 9–10, $p < 0.05$, unpaired t test) when IC_{50} values were assessed for both compounds in the same experiment. The exact nature of the hydrogen-bonding environment is difficult to predict using

Table 2. pH Dependence for 93-31 IC_{50} of Selected Mutants of GluN1/GluN2B and Estimates of the Corresponding Solution versus Intraprotein pKa Values

Mutation	Solution pKa[a]	Intraprotein pKa* [a]	IC_{50} μM, Maximum % Inhibition at pH 7.6 (N)[b]	IC_{50} μM, Maximum % Inhibition at pH 6.9 (N)[b]	IC_{50}(7.6)/IC_{50}(6.9)
GluN2B[c]	–	–	1.8 μM, 76% (32)	0.19 μM, 83% (23)	9.5
GluN2B(D77A)	3.9	4.1	68 μM, 100%[d] (6)	5.9 μM, 93% (10)	12
GluN2B(K79A)	10.5	11.1	2.7 μM, 70% (8)	0.36 μM, 68% (10)	7.5
GluN2B(D104A)	3.9	4.7	110 μM, 100% (6)	19 μM, 100% (8)	5.8
GluN2B(E106A)	4.3	7.0	11 μM, 96% (7)	4.3 μM, 80% (9)	2.6
GluN2B(E106Q)	4.3	7.0	8.7 μM, 70% (8)	3.2 μM, 91% (8)	2.7
GluN2B(E106D)	4.3	7.0	4.4 μM, 91% (7)	1.1 μM, 85% (7)	4.0
GluN2B(D113A)	3.9	5.8	6.2 μM, 55% (9)	1.3 μM, 55% (7)	4.8
GluN2B(D136A)	3.9	4.8	5.4 μM, 85% (10)	0.55 μM, 74% (9)	9.8
GluN2B(K137A)	10.5	7.8	28 μM, 95% (7)	1.8 μM, 84% (10)	16
GluN2B(D138A)	3.6	3.3	2.6 μM, 77% (10)	0.18 μM, 86% (8)	14
GluN2B(D206A)	3.6	3.1	82 μM, 100% [d] (9)	83 μM, 100% [d] (7)	1.0
GluN2B(D210A)	3.6	3.8	13 μM, 52% (7)	3.9 μM, 69% (11)	3.3
GluN2B(D211A)	3.6	2.9	7.1 μM, 75%, (9)	2.5 μM, 89% (24)	2.8
GluN2B(K215A)	10.5	9.7	3.3 μM, 63% (13)	0.29 μM, 71% (8)	11
GluN2B(K234A)	10.5	9.8	21 μM, 80% (6)	3.9 μM, 89% (12)	5.4
GluN2B(E235A)	4.3	5.1	120 μM, 100%[d] (13)	80 μM, 100%[d] (7)	1.5
GluN2B(E235Q)	4.3	5.1	1.2 μM, 67% (12)	0.49 μM, 73% (8)	2.4
GluN2B(E235D)	4.3	5.1	0.93 μM, 80% (7)	0.22 μM, 76% (8)	4.2
GluN2B(E106Q,E235Q)	–	–	9.2 μM, 71% (7)	4.7 μM, 98% (4)	2.0
GluN2B(E106D,E235D)	–	–	2.2 μM, 79% (8)	1.1 μM, 74% (10)	2.0
GluN2B(E236A)	4.3	5.7	6.9 μM, 90% (10)	0.85 μM, 93% (18)	14
GluN1(R115A)	12.5	11.2	4.3 μM, 68% (15)	2.8 μM, 83% (12)	1.5
GluN1(D130A)	3.9	4.7	3.7 μM, 76% (8)	2.4 μM, 96% (10)	1.5
GluN1(K131A)	10.5	10.5	2.3 μM, 86% (7)	0.51 μM, 89% (7)	4.6
GluN1(H134A)[e]	6.0	3.2	0.7 μM, 157%[e] (17)	0.8 μM, 147%[e] (14)	0.9
GluN1(G112A)	–	–	4.6 μM, 73% (16)	1.2 μM, 80% (29)	3.8
GluN1(G112V)	–	–	18.7 μM, 85% [f] (7)	18.5 μM, 85%[f] (5)	1.0

[a]pKa values in free solution were compared to those derived from the GluN1/GluN2B ATD heterodimer solved at pH 7.5 with coordinates from PDB code 3QEL. *Intraprotein pKa predicted with PropKA 3.1(Olsson, 2011).

[b]IC_{50} values to two significant figures for inhibition of GluN1/GluN2B expressed in *Xenopus* oocytes were determined as described in the Experimental Procedures from composite 93-31 inhibition curves. The fitted maximal inhibition is given as percent, and the number of oocytes is given in parentheses.

[c]Data for compound 93-31 are reproduced from Table 1 and included here to facilitate comparison.

[d]Maximum inhibition was fixed to be 100%.

[e]This mutation converted 93-31 into a potentiator, with EC_{50} and maximal potentiation given.

[f]Maximum inhibition was fixed to be 85%.

docking programs, due to the absence of solvent and the multiplicity of protonation states. However, these results suggest that a favorable network of interactions may exist under acidic conditions between 93-31, Glu106, and Glu235. Consistent with this idea, NP10075, a pH-sensitive GluN2B-selective antagonist recently reported by Wang et al. (2014), docks in poses similar to those of 93-31 (Figure S3). Whereas NP10075 lacks the side chain of the 93-series that exploits the GluN1 tunnel, the bulky piperazine moiety nevertheless appears to orient the hydroxyl to interact with Glu106 in similar fashion to 93-31. This raises the idea that the pH sensitivity of NP10075 also reflects an interaction with the pH-sensitive dicarboxylate Glu106:Glu235 dimer.

Glu235 also lies in close proximity to Glu106 in the ligand-bound structure such that it could be responsible for raising the pKa of Glu106, leading to protonation at pH 6.9. To directly assess this prediction, we mutated all residues within 12 Å of the ifenprodil binding pocket to alanine, and measured the pH sensitivity of 93-31 potency. A large number of these mutations modestly perturbed the pH sensitivity of 93-31 inhibition (Table 2). However, among these, three GluN2B mutations (E106A, E206A, and E235A) eliminated the pH dependence of inhibition by 93-31, two of which show pH-sensitive conformations. The third residue (Glu206) is close enough to interact with Glu235, and replacement with a neutral residue may render

the local microenvironment favorable to maintenance of a negative charge on Glu106 and Glu235 at both pH values, preventing carboxylic acid dimer formation. Furthermore, both E206A and E106A substantially increased IC_{50} values at both pH values, perhaps reflective of a larger structural rearrangement that reduces 93-31 binding, thereby obscuring the pH effect.

Mutations at Glu106 and Glu235 produce modest effects on inhibition by 93-31 at pH 7.6, but stronger effects at pH 6.9. For example, GluN2B(E106A) increased the IC_{50} by 6-fold at pH 7.6 (11 μM) and by 23-fold at pH 6.9 (IC_{50} 4.3 μM). This is consistent with the idea that the potency of 93-31 could be dependent on the ionization state of Glu106, which, given the shift of its pKa, can be influenced by modest reduction in pH to 6.9 in the ischemic penumbra. We mutated this glutamate to glutamine to remove the ionizable carboxylate, and found that GluN2B(E106Q) shifted IC_{50} values more at pH 6.9 (17-fold) than at pH 7.6 (5-fold). Isosteric replacement of ionizable Glu with the protonated Gln presumably allows for a weak interaction between these residues at both pH values, partially eliminating the pH sensitivity. The double mutant GluN2B(E106Q,E235Q) showed the same effect as GluN2B(E106Q) alone (Table 2), suggesting that the main effect is mediated by Glu106. We predicted that shortening the side chain by converting glutamate to aspartate should also diminish the pH sensitivity if there are tight geometrical constraints on interactions between the two closely spaced glutamates. Consistent with this prediction, introduction of an aspartate in GluN2B(E106D) diminished the pH sensitivity of 93-31 inhibition to 2.4- and 5.8-fold for pH 7.6 and 6.9, respectively. Again, introduction of the double mutation GluN2B (E106D,E235D) resulted in an effect similar to GluN2B(E106D), suggesting Glu106 was the primary determinant. In summary, the differential position of Glu235 in the crystal structures solved at two pH values, the predicted shift in the Glu106:Glu235 dimer pKa*'s to values that change ionization as pH drops to 6.9, and the mutagenesis-induced change in pH sensitivity of 93-31 all suggest that Glu106 and Glu235 are candidates for controlling the pH sensitivity of 93-31 binding.

Potential Role of Other pH-Sensitive Binding-Site Residues

Several other acidic residues revealed substantially altered pKa values (Asp113, Lys137, and His134) or pH sensitivity (Asp206, Asp 210, and Asp211). GluN2B-Asp113 (pKa 5.8; Figure 2D) is close enough to form hydrogen bonds with the backbone amide hydrogen of GluN2B-Asp138 and the side chain of GluN2B-Ser141, and form a water-bridged interaction with GluN1-Tyr109. The predicted increase in pKa* for Asp113 could lead to fractional protonation under acidic conditions, which should alter the hydrogen bonding networks associated with GluN2B-Asp138 and GluN1-Tyr109. If the interaction is reciprocal and favors protonation of a fraction of Asp113 side chains, binding of 93-31 may be facilitated and stabilize the protonated state (i.e., raising the pKa). In this context, it may be noted that a string of Glu and Asp side chains form a negatively charged layer above the ifenprodil binding site (Figure 4A; GluN2B residues 236, 235, 104, 106, 136, and 113). Each of these residues experiences an increase in predicted pKa* relative to the free solution. The proposed Glu106:Glu235 pH sensor resides at one end of the layer. Any change in the protonation state of the dicarboxylate sensor could significantly influence this cluster of residues, allowing them to serve as a trigger for perturbation of local conformation and ionization state as part of the binding event. The close clustering of acidic residues has been implicated in the pH-sensing mechanism of the acid sensing ion channel-1 protein (Jasti et al., 2007). Similarly, there is a cluster of cationic GluN1 residues (343, 115, and 134; Figure 3A), the intraprotein pKa*s of which are predicted to decrease relative to free solution. Thus, the ligand resides between electrostatic layers of opposite charge, in a situation that may render ligand binding sensitive to changes in both ligand configuration and pH. The complexity of this region is highlighted by the mutation of GluN1-His134 to Ala, which converts 93-31 into a pH-insensitive positive allosteric modulator (Table 2).

Three mutations at residues near the GluN1/GluN2B interface (Asp206, Asp210, and Asp211) substantially altered the pH sensitivity of 93-31 inhibition (Table 2). GluN2B-Asp210 is close enough to interact with GluN1-Arg323. Similarly, GluN2B-Asp206 can interact with GluN1-Lys322, although the large decrease in potency at both pH 6.9 and 7.6 for GluN2B(D206A) suggests a larger disturbance of 93-31 binding. Lastly, Asp211 interacts with the positive N terminus of an α helix. Whereas the pKa predictions suggest pH-induced effects are unlikely at pH 6.9, protonation of any of these residues could weaken or abolish their respective interactions.

Neuroprotection by pH-Dependent GluN2B-Selective Antagonists

In order to test the hypothesis that a pH drop associated with ischemic tissue engages the pH-sensitive enhanced potency of GluN2B antagonists in vivo for neuroprotection, we evaluated the efficacy of the pH-sensitive inhibitors on infarct volume following transient occlusion of the middle cerebral artery (MCAo) in mice. We selected two structural isomers that differed only in the N-alkyl chain, compound 93-31, which contains an *n*-butyl and is pH sensitive, and compound 93-97, with less pH sensitivity and an *iso*-butyl substituent (Table 1). Each compound was administered by intracerebroventricular (i.c.v.) injection directly into the lateral ventricle 20 min prior to initiation of transient focal ischemia by MCAo. Figures 5A and 5B shows both the method of determining the infarct volume and that i.c.v. administration of 93-31 produced dose-dependent and robust 59% reduction in infarct volume compared to vehicle. However, compound 93-97 was ineffective as a neuroprotectant with no reduction in infarct volume, consistent with our in vitro studies showing that the potency of 93-97 is relatively insensitive to pH. That is, 93-97 potency is similar to that of 93-31 at physiological pH 7.35 (93-31 IC_{50} = 2.2 μM, 93-97 IC_{50} = 4.8 μM, n = 5–6), but not enhanced sufficiently at pH 6.9 (Table 1) to render it efficacious in penumbral regions (Figures 5A and 5B).

Prior generations of competitive and noncompetitive NMDAR antagonists cause a variety of off-target and on-target adverse effects that prevented clinical development, including motor dysfunction, cognitive impairment, and psychotomimetic effects including hallucinations, paranoia, disorganized thought, and blunted affect (Lees et al., 2000; Sacco et al., 2001; Diener et al., 2002; Rowland, 2005; Wood, 2005; Muir, 2006; Blagrove

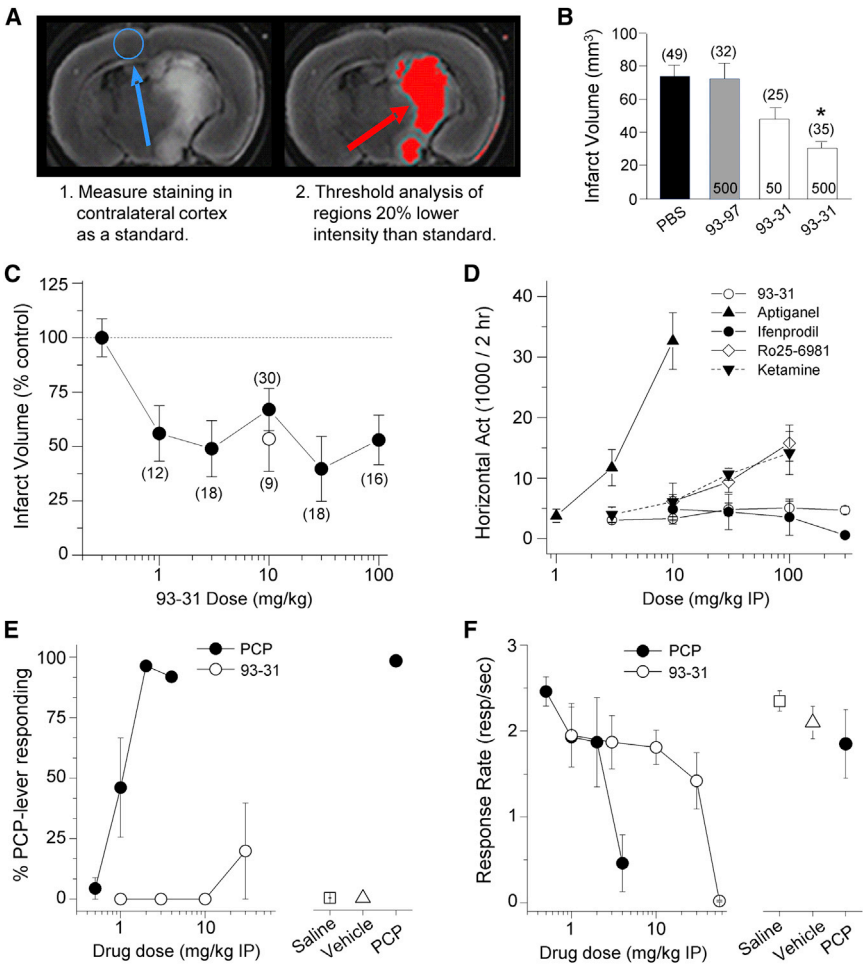

Figure 5. 93-31 Is Neuroprotective against Transient Ischemia without Side Effects

(A) (Left panel) A single mouse brain section (2 mm) obtained 24 hr post-ischemia and stained with TTC as described in Experimental Procedures. (Right panel) The same mouse section is shown with areas for which the TTC intensity that is 20% below threshold selected from contralateral cortex (blue circle) is shown as red.

(B) Summary of MCAo infarct volume results from treatment groups injected with (in pmols) 93-31 (50, 500), or 93-97 (500) compound by i.c.v., or an equivalent PBS volume (vehicle) 20 min before MCAo. *$p < 0.005$ (ANOVA, Tukey post hoc test), number of mice/group indicated.

(C) Dose-response curve for 93-31 administered IP 20 min preceding MCAo in mice (solid symbols) or 30 min after MCAo reperfusion (open symbol). Infarct volume was determined by TTC staining as described in (A) and Experimental Procedures. Number of mice/group is indicated; all measurements were significantly different ($p < 0.05$) from vehicle (ANOVA and Dunnett's test).

(D) Horizontal locomotor activity (cumulative 2 hr period) following i.p. administration of the indicated drug and dose in rats is shown. n = 6–8. Higher doses of Ro 25-6981 and ketamine were not tested.

(E) 93-31 failed to produce PCP-associated lever responding in rats trained to discriminate PCP from saline. n = 6 for all except 4 mg/kg PCP (n = 3) and 30 mg/kg 93-31 (n = 5).

(F) The highest dose tested in the PCP discrimination study, 56 mg/kg, significantly suppressed response rates in the same subjects, suggesting behaviorally active doses were tested (see Experimental Procedures). n = 6 for all. All data presented as mean ± SEM. See also Figure S4 and Table S5.

et al., 2009). Although the GluN2B-selective class of antagonists are better tolerated than competitive antagonists or channel blockers, they are not necessarily free from on-target side effects (Chaperon et al., 2003; De Vry and Jentzsch, 2003; Yurkewicz et al., 2005; Nicholson et al., 2007; Preskorn et al., 2008; Nutt et al., 2008). Our working hypothesis is that enhanced pH sensitivity should increase the therapeutic ratio (TR) to enable efficacious dosing for neuroprotection in ischemic penumbral regions surrounding the infarct (pH 6.9), with reduced inhibition of GluN2B receptors in normal brain (pH 7.4). That is, the pH sensitivity of the NMDAR antagonist should lower the potential for on-target side effects. To determine a TR (the ratio of ED_{50} for efficacy versus side-effect studies) for 93-31 as a neuroprotectant, we completed additional MCAo studies in which 93-31 showed potent neuroprotection during ischemia, reducing infarct volumes up to 50% with an apparent ED_{50} value of <1 mg/kg (Figure 5C). For these studies, 93-31 was dosed intraperitoneally (i.p.) 20 min prior to transient ischemia by MCAo. Further, administration of 93-31 (10 mg/kg IP) 30 min post-MCAo also reduced infarct volume to a similar extent (open symbol, Figure 5C). PK studies in surrogate mice support drug exposures in brain consistent with potency at low pH (Table S5; Supplemental Experimental Procedures).

We subsequently made three measurements of potential on-target dose-limiting side effects. First, we evaluated effects of 93-31 on locomotor activity and found no significant effects on horizontal activity at doses up to 300 mg/kg compared to vehicle (4,415 ± 479, n = 24) over 2 hr following 1 hr habituation, in contrast to the channel blockers aptiganel and ketamine. The GluN2B-selective antagonists ifenprodil and Ro 25-6981 reduced and increased locomotor activity, respectively, at high doses (Figure 5D). Second, we evaluated the effects of 93-31 in a rotorod test. Both the noncompetitive NMDAR antagonist (+)MK-801 and ifenprodil impaired performance, exhibiting strong reductions in latency to fall (vehicle 140 ± 13 s, n = 12; 0.6 mg/kg [+]MK-801 3 ± 2 s, n = 5; 30 mg/kg ifenprodil 35 ± 6 s, n = 5). By contrast, there was no significant effect of 93-31 (108 ± 14 s, n = 6) nor 93-97 (117 ± 19 s, n = 6) on rotorod performance at 30 mg/kg (Figure S4). Third, we tested the ability of GluN2B-selective NMDAR blockers to be recognized by rodents trained to discriminate the noncompetitive channel blocker PCP from saline. Trained animals were administered 93-31, PCP, or saline on test days. Interestingly, 93-31 failed to substitute for PCP in this paradigm (Figure 5E), suggesting this compound is devoid of psychotomimetic effects at the doses tested. At the highest dose (56 mg/kg), there was a significant

depression in lever-pressing behavior, indicating that behaviorally active doses were tested and therefore the lack of PCP-like effects was not attributable to an inadequate dose range (Figure 5F). Of these four behaviors (locomotor activity, rotorod, PCP discrimination, and lever pressing), we identified only one in which 93-31 caused significant effects at doses of 30 mg/kg or higher. From the ED_{50} for neuroprotection (<1 mg/kg) we calculate a TR for neuroprotection in rodents following IP administration of >30 for the pH-sensitive 93-31 GluN2B inhibitor, a value considerably higher than that estimated for neuroprotection in the literature for ifenprodil and dizolcilpine (TR $\leq$ 1; Hatfield et al., 1992; Bertorelli et al., 1998; Dawson et al., 2001; Xiao et al., 2004) and CP-101,606 (TR ~4; Yang et al., 2003, Nicholson et al., 2007).

DISCUSSION

Two important findings emerge from this study. First, these data provide molecular insight into the nature of inhibition produced by therapeutically relevant GluN2B-selective modulators that bind to the GluN1/GluN2B heterodimer interface of the amino terminal domain (Karakas et al., 2011; Burger et al., 2012; Karakas and Furukawa 2014; Lee et al., 2014). Our data suggest that changes in the 93-31 association/dissociation rates at acidic pH reflect an altered configuration around the binding pockets when ionizable residue(s) in helix-3 and helix-8 are protonated. The juxtaposition of ionizable side chains by tertiary protein structure has been suggested to shift intraprotein pKa values (Harris and Turner 2002; Jasti et al., 2007; Ritschel et al., 2009; Bombarda and Ullmann 2010; Sussman et al., 2013), creating a carboxylate-based pH sensor for ligand binding within the amino-terminal domain that docking studies suggest directly interacts with 93-31. Interestingly, an interacting carboxylate pair has recently been suggested to form the pH sensor of a Ca^{2+} leak channel (Chang et al., 2014). While the Ca^{2+} leak channel dicarboxylate pair does not form the classic reciprocal hydrogen bonding of a carboxylic acid dimer, it nonetheless alternates between multiple states with varying pH, including protonation of both side chains. In addition to ionization of the GluN2B glutamate residues impacting 93-31 binding rates, it is also possible that occupancy of the binding site by different propanolamines (Table 1) can differentially impact position and pKa of these residues. Whereas data suggest that most of the pH sensitivity is derived from changes in binding rates of 93-31, it is possible that some pH sensitivity reflects the ability of 93-31 binding to bring about downstream protein conformation changes that govern efficacy (Low et al., 2003; Gielen et al., 2008).

Second, the development of GluN2B inhibitors with pH-dependent potency is important, considering problems with past clinical programs centered on neuroprotection by NMDAR antagonists. Data presented here show that NMDAR antagonists can be designed that provide enhanced receptor blockade during a decrease in extracellular pH, resulting in neuroprotection in acidic ischemic tissue without untoward side effects. This is because the increased potency in ischemic tissue reduces the concentration needed for neuroprotection below that which will cause effects at normal pH in healthy brain. Decreased extracellular pH universally accompanies ischemic injury and TBI (Mutch and Hansen, 1984; Smith et al., 1986; Nedergaard et al., 1991; Katsura et al., 1992; Katsura and Siesjo, 1998), suggesting this strategy may be applicable to acute neurodegeneration under a wide range of insults. Our application of this concept to the well-tolerated class of GluN2B-selective NMDAR antagonists further increases the likelihood that antagonists with these properties will be clinically viable for indications with synaptic or interstitial acidic pH changes. This context dependence enhances the TR for such pH-sensitive compounds. We calculate from the effects on infarct volume following ischemia and from the dose-effect relationship in healthy animals using PCP discrimination studies that 93-31 has a TR greater than 30, which is higher than that which can be calculated from the literature for GluN2B-NMDAR antagonists acting as neuroprotectants (see above).

In light of these data, the results of clinical studies with CP-101,606, which nearly reached significance for a TBI trial despite a lengthy time window for drug administration (8 hr) postinjury, are encouraging. CP-101,606 (Mott et al., 1998) and other GluN2B antagonists lack substantial pH sensitivity (Table S6), and thus it is intriguing to speculate that a compound with similar actions as CP-101,606 but with the additional enhanced pH sensitivity might be clinically successful. If the concept of context-dependent inhibition is coupled with modern clinical trial designs that allow rapid, blinded trials by first responders within hours of ischemic onset or traumatic insult (Saver 2013), there is excellent likelihood that the well-known neuroprotective potential of NMDAR antagonists can impact clinical outcomes in ischemia and TBI. This proof-of-concept molecule demonstrates the utility of this strategy and creates a strong precedent for exploiting the pH dependence of the GluN2B class of NMDAR antagonists for brain injury involving overactivation of NMDARs and extracellular acidification.

EXPERIMENTAL PROCEDURES

Voltage-Clamp Recordings from Transfected HEK Cells

HEK293 cell preparation and transfection were conducted (see Supplemental Experimental Procedures) as described previously (Yuan et al., 2009). Following transfection of GluN1-1a (hereafter GluN1, GenBank U11418) and GluN2B (GenBank U11419), whole-cell voltage-clamp recordings were conducted on transiently transfected HEK cells using an Axopatch 200B amplifier (Molecular Devices, Union City, CA, USA). Current responses were digitized at 40 kHz by pClamp10 software (Molecular Devices). Recordings were filtered at 8 kHz using an eight-pole Bessel filter (−3 dB; Frequency Devices, Haverhill, MD, USA). Thin-walled borosilicate glass capillary tubes (World Precision Instruments, catalog number TW-150F-4, Hamden, CT, USA) were used to form recording micropipettes for whole-cell currents. All recording micropipettes were filled with an internal solution containing (in mM) 110 D-gluconic acid, 110 CsOH, 30 CsCl, 5 HEPES, 5 BAPTA, 4 NaCl, 2 $MgCl_2$, 2 NaATP, 0.5 $CaCl_2$, and 0.3 NaGTP (pH 7.35). Cells were bathed at 23°C in external solution that contained (in mM) 150 NaCl, 10 HEPES, 3 KCl, 0.5 $CaCl_2$, 0.01 EDTA, and 30 D-mannitol at pH 7.6 or pH 6.9. All recording solutions were made from external solution and recordings were performed at holding potentials of −60 mV. Rapid solution exchange for macroscopic recordings was accomplished with a two-barrel theta glass pipette controlled by a piezoelectric translator (Burleigh Instruments, Fishers, NY); 10%–90% open tip solution exchange times were under 1 ms, and solution exchange around the whole cell was under 5 ms (Vance et al., 2011). Assuming 93-31 follows the law of mass

action, the exponential time course for the onset of inhibition should have a tau described by Equation (1),

$$Tau_{ONSET} = 1/(k_{ON}[concentration] + k_{OFF}), \quad \text{(Equation 1)}$$

where k_{ON} and k_{OFF} are the microscopic association and dissociation rate constants. From this relationship we can determine the association rate (k_{ON}) from the slope of linear plot of $1/Tau_{ONSET}$ and concentration (Figure 1D) and the dissociation rate (k_{OFF}) from the intercept ($K_D = k_{OFF}/k_{ON}$).

Two Electrode Voltage-Clamp Recordings from *Xenopus* Oocytes

All protocols involving animals were approved by the Emory University and Virginia Commonwealth University IACUC. Stage V–VI *Xenopus laevis* unfertilized oocytes purchased from Ecocyte (Austin, TX), and were injected with 3–5 ng of GluN1 and 7–10 ng of GluN2B cRNAs, and incubated in Barth's solution at 18°C. Two electrode voltage-clamp recordings were made 2–7 days postinjection at a holding potential of –40 mV using two Warner OC725B two-electrode voltage-clamp amplifiers (23°C). Oocytes were perfused with a solution of (in mM) 90 NaCl, 1 KCl, 10 HEPES, 0.01 EDTA, and 0.5 $BaCl_2$; pH was adjusted to 7.6 by addition of NaOH, and subsequently lower pH values by addition of HCl to ensure constant concentration of Na^+ in all solutions. Concentration-response inhibition curves were obtained by bath application of increasing concentrations of antagonist in the presence of 50–100 μM L-glutamate and 30 μM glycine until steady-state conditions were reached (1–6 min typically, 15 min in some cases). Recordings were made from three to ten oocytes per experiment from two to six experiments. The percent responses for the composite data were fit by Equation (2),

$$Percent\ Response = (100 - minimum) \Big/ \left(1 + ([concentration]/IC_{50})^{nH}\right) + minimum, \quad \text{(Equation 2)}$$

where *minimum* is the residual percent response in saturating concentration (constrained to ≥ 0) of the experimental compounds, IC_{50} is the concentration of antagonist that causes half maximal inhibition, and *nH* is a slope factor of the inhibition curve.

Triheteromeric GluN1/2A/2B receptors were expressed in *Xenopus* oocytes using the constructs and method described in Hansen et al. (2014) (see Supplemental Experimental Procedures).

Docking of 93-Series Compounds

Compounds 93-31, 93-97, and NP10075 were built in Maestro 9.2 (Schrodinger suite) and docked using the OPLS2005 force field and Glide Induced Fit docking protocol (Sherman et al., 2006). The atomic coordinates for GluN1/GluN2B amino terminal domain cocrystallized with ifenprodil was used as the input structure (3QEL; Karakas et al., 2011). The binding site was defined by residues within 5 Å of ifenprodil, which were treated as flexible. A maximum of 100 poses per ligand was generated. Both *N*-protonated stereoisomers and the unprotonated form were docked. The unprotonated forms were docked with *N*-inversion enabled. All poses were also subsequently scored with MM-GBSA binding energy calculations (Prime version 3.1). VMD 1.9 (Humphrey et al., 1996) was used for visualization, while prediction of altered pKa values was carried out with the VMD PropKa plugin (Olsson 2011). The semiempirical PM6 electrostatic potential evaluation of the GluN1/GluN2B ligand binding site and the associated protein side chains was performed with Spartan 10, version 1.1.0., from Wavefunction Inc. (Young 2001; http://www.wavefun.com/products/products.html; accessed October 9, 2013).

In Vivo Models of Transient Focal Ischemia

Transient focal cerebral ischemia (30 min) was induced in mice by intraluminal middle cerebral artery occlusion (MCAO; Junge et al., 2003). Male C57BL/6 mice (3–5 months old, Jackson Labs) were anesthetized with 2% isoflurane in 98% O_2. We avoided the use of ketamine, given its confounding neuroprotective channel-blocking actions on NMDARs (Hamill et al., 2009). The rectal temperature was monitored and mouse temperature maintained at 37°C (range 36.5–37.5) with a homeothermic blanket. Blood pressure was not monitored or controlled. Relative changes in regional cerebral blood flow were monitored with a laser Doppler flowmeter (Perimed); the Doppler probe was glued to the skull 2 mm posterior and 4–6 mm lateral of the bregma. Only animals with reduction in blood flow to 20% and clear recovery of blood flow were included in the study. An 11 mm 5-0 Dermalon or Look (SP185) black nylon nonabsorbable suture with the tip flame rounded was introduced for 30 min into the left internal carotid artery through the external carotid artery stump until monitored cerebral blood flow was reduced <20% (at 10.5–11 mm of suture insertion). Only animals with sustained reduction in blood flow to <20% for 30 min and clear recovery of blood flow to >90% following removal of the intraluminal suture were included. After 24 hr, the brain was removed and cut into 2 mm sections. The lesion was identified with 2% 2,3,5-triphenyltetrazolium chloride (TTC) in PBS at 37°C for 20 min and the infarct area measured using NIH IMAGE (Scion Corporation, Beta 4.0.2 release). The area of the lesion, as identified by digital threshold reductions in TTC staining 20% lower than intensity in contralateral cortex, was manually outlined and the cubic volume of the infarct size determined. A ratio of the contralateral to ipsilateral hemisphere section volume was multiplied by the corresponding infarct section volume to correct for edema. Drug was administered by intraperitoneal (i.p., 3 mL/kg) or by i.c.v. (1 ul) injection 10 min before initiation of surgery (i.e., 20 min before vessel occlusion) or 30 min after removal of the intraluminal suture. I.c.v. injections were made into the right ventricle (2 mm post., 1 mm lat. of the bregma, needle inserted 3 mm). Compound was formulated in 1:1 DMSO:phosphate buffered saline (pH 7.4) for IP injection and 1:10 DMSO:phosphate buffered saline (pH 7.4) for i.c.v. Those performing the surgical procedure and analysis were blinded to the identity of the treatment.

Measurement of Locomotor Activity, Rotorod Activity, and PCP Discrimination

Male Sprague-Dawley rats (100–150 g) were placed in activity monitoring boxes for a 1 hr habituation period prior to drug testing. At 1 hr, monitoring was interrupted to inject animals IP with various doses of drug in 50% v/v DMSO:saline. Animals were returned to the cage, and total locomotor activity was monitored for the next 2 hr. The total number of light beam breaks in the cage (horizontal and vertical) was automatically determined by a computer and results averaged for each drug. An ANOVA followed by Dunnett's test was used to compare total horizontal activity of drug doses to vehicle controls.

For rotorod, male C57BL/6 mice (>90 days old) were tested using a four-chamber Rotamax 4/8 rotorod (Columbus Instruments, Columbus, OH). The test was initiated by placing mice on a rotating rod (5 rpm) that was 3.8 cm diameter by 8 cm wide and suspended 30 cm from the floor of a chamber. After 10 s the rotation was accelerated from 5 to 35 rpm over a 5 min period. The latency to fall (sec) was recorded automatically with a light-activated sensor in the bottom of the chamber. Animals were trained four times with an intertrial interval of 25 min, each day for 2 days. On day 3 mice were randomly assigned to groups and administered compound or vehicle (i.p.; 47.5% DMSO, 47.5% saline, 5% DMA). Twenty minutes after drug administration the mice were tested as before with an intertrial interval of 25 min and latency to fall recorded. Those performing the study were blinded to the identity of the treatment group.

To evaluate the psychotomimetic effects of the test compounds, six adult male Sprague Dawley rats (Charles River, Wilmington, DE) were trained to discriminate administration of 2.0 mg/kg PCP from saline injections (Balster and Willetts 1988). They were singly housed with free access to water under a 12 hr light/dark cycle. Subjects were maintained at 85%–90% free feeding weight with food access (Harlan Teklad Rodent Diet, Williamston, IL) limited to postsession periods to motivate lever pressing for food. The subjects were trained daily (Monday through Friday) in 30 min sessions in standard two-lever operant conditioning chambers (MedAssociates, St. Alban, VT). Completion of 32 consecutive responses (fixed ratio 32; FR 32) on the appropriate lever resulted in reinforcement with delivery of a 45 mg food pellet (P.J. Noyes Company, Inc., Lancaster, NH). Responding on the incorrect lever reset the FR count toward pellet delivery. PCP and saline were administered IP under a double alternation schedule (e.g., drug, drug, saline, saline) 15 min prior to the beginning of the session. During sessions, a white stimulus light located centrally above each lever was illuminated. Test

sessions were conducted up to twice weekly when the subjects met the following criteria on the four preceding training sessions (two PCP and two saline): (1) first FR completed on the correct lever, and (2) greater than 85% correct lever responding over the entire session. During test sessions, completion of 32 consecutive responses on either lever resulted in the delivery of food.

Rats were tested at 93-31 doses of 1, 3, 10, 30, and 56 mg/kg administered IP, 30 min presession; various doses of PCP were tested in the same animals for comparison. Data were evaluated by calculating the mean percentage of responses on the PCP-associated lever and the overall mean response rate. For sessions in which a subject's responding was less than 0.05 resp/s, the percent PCP lever responding was excluded from determination of the group mean. Full substitution for PCP was defined as greater than 80% PCP lever responding, while partial substitution was defined as producing between 20% and 80% PCP lever responding.

Chemistry

The synthetic reaction schemes for all 93-series compounds can be found in Tahirovic et al. (2008).

Statistics

Values presented are mean ± SEM, and are compared using Student's paired or unpaired t test, and ANOVA where appropriate. The level of significance was chosen as 0.05.

SUPPLEMENTAL INFORMATION

Supplemental Information includes four figures, six tables, and Supplemental Experimental Procedures and can be found with this article online at http://dx.doi.org/10.1016/j.neuron.2015.02.008.

AUTHOR CONTRIBUTIONS

H.Y. designed and performed electrophysiology experiments, analyzed data, and wrote the paper. G.W. and J.P.S. performed molecular dynamic simulations, ligand docking, and homology modeling and wrote the paper. S.J.M. designed and performed pharmacology experiments in *Xenopus* oocytes and in vivo experiments, analyzed the data, and wrote the paper. K.L.N. designed and performed behavioral experiments, analyzed the data, and wrote the paper. S.A.S. designed and performed pharmacology experiments in *Xenopus* oocytes, analyzed the data, and wrote the paper. P.L. performed pharmacology experiments in *Xenopus* oocytes and in vivo experiments, and analyzed the data. Y.A.T., T.G., and D.S.M. synthesized compounds and wrote the paper. L.J.W. provided structural insight on NP10075. D.C.L. supervised the compounds synthesis and wrote the paper. S.F.T. designed experiments, performed in vivo experiments, analyzed data, wrote the paper, and supervised the project.

ACKNOWLEDGMENTS

This work was supported by NINDS (NS036654 ST), by ATDC (ST), EmTech Bio (RD). We thank Hiro Furukawa for critical comments on the manuscript, and Phuong Le, Jing Zhang, and Anel Tankovic for excellent technical assistance. We thank Ray Dingledine (NS36604) for early contributions and discussion. Several of the authors (Y.A.T., J.P.S., S.J.M., S.F.T., L.J.W., and D.C.L.) are coinventors of patented and patent-pending technology related to glutamate receptors, have an equity position (J.P.S., D.C.L., and S.F.T.), are board members (D.C.L.), paid consultants (S.F.T.), current employees (S.J.M.), or former employees (P.L., Y.A.T., and L.J.W.) for a company (NeurOp Inc) that has licensed this technology.

Received: September 11, 2014
Revised: January 12, 2015
Accepted: January 29, 2015
Published: February 26, 2015

REFERENCES

Albers, G.W., Goldstein, L.B., Hall, D., and Lesko, L.M.; Aptiganel Acute Stroke Investigators (2001). Aptiganel hydrochloride in acute ischemic stroke: a randomized controlled trial. JAMA *286*, 2673–2682.

Allen, F.H. (2002). The Cambridge Structural Database: a quarter of a million crystal structures and rising. Acta Crystallogr. B *58*, 380–388.

Balster, R.L., and Willetts, J. (1988). Receptor mediation of the discriminative stimulus properties of phencyclidine and sigma-opioid agonists. Psychopharmacol. Ser. *4*, 122–135.

Banke, T.G., Dravid, S.M., and Traynelis, S.F. (2005). Protons trap NR1/NR2B NMDA receptors in a nonconducting state. J. Neurosci. *25*, 42–51.

Benveniste, M., and Mayer, M.L. (1992). Effect of extracellular pH on the potency of N-methyl-D-aspartic acid receptor competitive antagonists. Mol. Pharmacol. *42*, 679–686.

Bertorelli, R., Adami, M., Di Santo, E., and Ghezzi, P. (1998). MK 801 and dexamethasone reduce both tumor necrosis factor levels and infarct volume after focal cerebral ischemia in the rat brain. Neurosci. Lett. *246*, 41–44.

Blagrove, M., Morgan, C.J.A., Curran, H.V., Bromley, L., and Brandner, B. (2009). The incidence of unpleasant dreams after sub-anaesthetic ketamine. Psychopharmacol. *203*, 109–120.

Bombarda, E., and Ullmann, G.M. (2010). pH-dependent pKa values in proteins—a theoretical analysis of protonation energies with practical consequences for enzymatic reactions. J. Phys. Chem. B *114*, 1994–2003.

Burger, P.B., Yuan, H., Karakas, E., Geballe, M., Furukawa, H., Liotta, D.C., Snyder, J.P., and Traynelis, S.F. (2012). Mapping the binding of GluN2B-selective N-methyl-D-aspartate receptor negative allosteric modulators. Mol. Pharmacol. *82*, 344–359.

Chang, Y., Bruni, R., Kloss, B., Assur, Z., Kloppmann, E., Rost, B., Hendrickson, W.A., and Liu, Q. (2014). Structural basis for a pH-sensitive calcium leak across membranes. Science *344*, 1131–1135.

Chaperon, F., Müller, W., Auberson, Y.P., Tricklebank, M.D., and Neijt, H.C. (2003). Substitution for PCP, disruption of prepulse inhibition and hyperactivity induced by N-methyl-D-aspartate receptor antagonists: preferential involvement of the NR2B rather than NR2A subunit. Behav. Pharmacol. *14*, 477–487.

Chenard, B.L., and Menniti, F.S. (1999). Antagonists selective for NMDA receptors containing the NR2B subunit. Curr. Pharm. Des. *5*, 381–404.

Choi, D.W., Koh, J.Y., and Peters, S. (1988). Pharmacology of glutamate neurotoxicity in cortical cell culture: attenuation by NMDA antagonists. J. Neurosci. *8*, 185–196.

Dawson, D.A., Wadsworth, G., and Palmer, A.M. (2001). A comparative assessment of the efficacy and side-effect liability of neuroprotective compounds in experimental stroke. Brain Res. *892*, 344–350.

De Vry, J., and Jentzsch, K.R. (2003). Role of the NMDA receptor NR2B subunit in the discriminative stimulus effects of ketamine. Behav. Pharmacol. *14*, 229–235.

Diener, H.C., AlKhedr, A., Busse, O., Hacke, W., Zingmark, P.H., Jonsson, N., and Basun, H.; Study group (2002). Treatment of acute ischaemic stroke with the low-affinity, use-dependent NMDA antagonist AR-R15896AR. A safety and tolerability study. J. Neurol. *249*, 561–568.

Ellrén, K., and Lehmann, A. (1989). Calcium dependency of N-methyl-D-aspartate toxicity in slices from the immature rat hippocampus. Neurosci. *32*, 371–379.

Farin, A., and Marshall, L.F. (2004). Lessons from epidemiologic studies in clinical trials of traumatic brain injury. Acta Neurochir. Suppl. (Wien) *89*, 101–107.

Gielen, M., Le Goff, A., Stroebel, D., Johnson, J.W., Neyton, J., and Paoletti, P. (2008). Structural rearrangements of NR1/NR2A NMDA receptors during allosteric inhibition. Neuron *57*, 80–93.

Gladstone, D.J., Black, S.E., and Hakim, A.M.; Heart and Stroke Foundation of Ontario Centre of Excellence in Stroke Recovery (2002). Toward wisdom from failure: lessons from neuroprotective stroke trials and new therapeutic directions. Stroke *33*, 2123–2136.

Hamill, C.E., Mannaioni, G., Lyuboslavsky, P., Sastre, A.A., and Traynelis, S.F. (2009). Protease-activated receptor 1-dependent neuronal damage involves NMDA receptor function. Exp. Neurol. *217*, 136–146.

Hansen, K.B., Ogden, K.K., Yuan, H., and Traynelis, S.F. (2014). Distinct functional and pharmacological properties of Triheteromeric GluN1/GluN2A/GluN2B NMDA receptors. Neuron *81*, 1084–1096.

Harris, T.K., and Turner, G.J. (2002). Structural basis of perturbed pKa values of catalytic groups in enzyme active sites. IUBMB Life *53*, 85–98.

Hatfield, R.H., Gill, R., and Brazell, C. (1992). The dose-response relationship and therapeutic window for dizocilpine (MK-801) in a rat focal ischaemia model. Eur. J. Pharmacol. *216*, 1–7.

Hatton, C.J., and Paoletti, P. (2005). Modulation of triheteromeric NMDA receptors by N-terminal domain ligands. Neuron *46*, 261–274.

Humphrey, W., Dalke, A., and Schulten, K. (1996). VMD: visual molecular dynamics. J. Mol. Graph. *14*, 33–38, 27–28.

Jasti, J., Furukawa, H., Gonzales, E.B., and Gouaux, E. (2007). Structure of acid-sensing ion channel 1 at 1.9 A resolution and low pH. Nature *449*, 316–323.

Junge, C.E., Sugawara, T., Mannaioni, G., Alagarsamy, S., Conn, P.J., Brat, D.J., Chan, P.H., and Traynelis, S.F. (2003). The contribution of protease-activated receptor 1 to neuronal damage caused by transient focal cerebral ischemia. Proc. Natl. Acad. Sci. USA *100*, 13019–13024.

Kaplan, J., Dimlich, R.V., Biros, M.H., and Hedges, J. (1987). Mechanisms of ischemic cerebral injury. Resuscitation *15*, 149–169.

Karakas, E., and Furukawa, H. (2014). Crystal structure of a heterotetrameric NMDA receptor ion channel. Science *344*, 992–997.

Karakas, E., Simorowski, N., and Furukawa, H. (2009). Structure of the zinc-bound amino-terminal domain of the NMDA receptor NR2B subunit. EMBO J. *28*, 3910–3920.

Karakas, E., Simorowski, N., and Furukawa, H. (2011). Subunit arrangement and phenylethanolamine binding in GluN1/GluN2B NMDA receptors. Nature *475*, 249–253.

Katsura, K., and Siesjo, B. (1998). Acid-base metabolism in ischemia. In pH and Brain Function, K. Kaila and B.R. Ransom, eds. (New York: Wiley-Liss), p. 563.

Katsura, K., Asplund, B., Ekholm, A., and Siesjö, B.K. (1992). Extra- and intracellular pH in the brain during ischaemia, related to tissue lactate content in normo- and hypercapnic rats. Eur. J. Neurosci. *4*, 166–176.

Kidwell, C.S., Liebeskind, D.S., Starkman, S., and Saver, J.L. (2001). Trends in acute ischemic stroke trials through the 20th century. Stroke *32*, 1349–1359.

Lee, C.H., Lü, W., Michel, J.C., Goehring, A., Du, J., Song, X., and Gouaux, E. (2014). NMDA receptor structures reveal subunit arrangement and pore architecture. Nature *511*, 191–197.

Lees, K.R., Asplund, K., Carolei, A., Davis, S.M., Diener, H.C., Kaste, M., Orgogozo, J.M., and Whitehead, J.; GAIN International Investigators (2000). Glycine antagonist (gavestinel) in neuroprotection (GAIN International) in patients with acute stroke: a randomised controlled trial. Lancet *355*, 1949–1954.

Leiserowitz, L., Harris, T.K., and Turner, G.J. (2002). Molecular packing modes. Carboxylic acids. Acta Crystallogr. B *53*, 85–98.

Low, C.M., Lyuboslavsky, P., French, A., Le, P., Wyatte, K., Thiel, W.H., Marchan, E.M., Igarashi, K., Kashiwagi, K., Gernert, K., et al. (2003). Molecular determinants of proton-sensitive N-methyl-D-aspartate receptor gating. Mol. Pharmacol. *63*, 1212–1222.

Macrae, C.F., Edgington, P.R., McCabe, P., Pidcock, E., Shields, G.P., Taylor, R., Towler, M., and van de Streek, J. (2006). Mercury: visualization and analysis of crystal structures. J. Appl. Cryst. *39*, 453–457.

Matsumoto, T., Obrenovitch, T.P., Parkinson, N.A., and Symon, L. (1990). Cortical activity, ionic homeostasis, and acidosis during rat brain repetitive ischemia. Stroke *21*, 1192–1198.

Mody, I., and MacDonald, J.F. (1995). NMDA receptor-dependent excitotoxicity: the role of intracellular Ca2+ release. Trends Pharmacol. Sci. *16*, 356–359.

Morris, G.F., Bullock, R., Marshall, S.B., Marmarou, A., Maas, A., and Marshall, L.F.; The Selfotel Investigators (1999). Failure of the competitive N-methyl-D-aspartate antagonist Selfotel (CGS 19755) in the treatment of severe head injury: results of two phase III clinical trials. J. Neurosurg. *91*, 737–743.

Mosley, C.A., Myers, S.J., Murray, E.E., Santangelo, R., Tahirovic, Y.A., Kurtkaya, N., Mullasseril, P., Yuan, H., Lyuboslavsky, P., Le, P., et al. (2009). Synthesis, structural activity-relationships, and biological evaluation of novel amide-based allosteric binding site antagonists in NR1A/NR2B N-methyl-D-aspartate receptors. Bioorg. Med. Chem. *17*, 6463–6480.

Mott, D.D., Doherty, J.J., Zhang, S., Washburn, M.S., Fendley, M.J., Lyuboslavsky, P., Traynelis, S.F., and Dingledine, R. (1998). Phenylethanolamines inhibit NMDA receptors by enhancing proton inhibition. Nat. Neurosci. *1*, 659–667.

Muir, K.W. (2006). Glutamate-based therapeutic approaches: clinical trials with NMDA antagonists. Curr. Opin. Pharmacol. *6*, 53–60.

Mutch, W.A., and Hansen, A.J. (1984). Extracellular pH changes during spreading depression and cerebral ischemia: mechanisms of brain pH regulation. J. Cereb. Blood Flow Metab. *4*, 17–27.

Narayan, R.K., Michel, M.E., Ansell, B., Baethmann, A., Biegon, A., Bracken, M.B., Bullock, M.R., Choi, S.C., Clifton, G.L., Contant, C.F., et al. (2002). Clinical trials in head injury. J. Neurotrauma *19*, 503–557.

Nedergaard, M., Kraig, R.P., Tanabe, J., and Pulsinelli, W.A. (1991). Dynamics of interstitial and intracellular pH in evolving brain infarct. Am. J. Physiol. *260*, R581–R588.

Nicholson, K.L., Mansbach, R.S., Menniti, F.S., and Balster, R.L. (2007). The phencyclidine-like discriminative stimulus effects and reinforcing properties of the NR2B-selective N-methyl-D-aspartate antagonist CP-101 606 in rats and rhesus monkeys. Behav. Pharmacol. *18*, 731–743.

Nutt, J.G., Gunzler, S.A., Kirchhoff, T., Hogarth, P., Weaver, J.L., Krams, M., Jamerson, B., Menniti, F.S., and Landen, J.W. (2008). Effects of a NR2B selective NMDA glutamate antagonist, CP-101,606, on dyskinesia and Parkinsonism. Mov. Disord. *23*, 1860–1866.

Olney, J.W. (1969). Brain lesions, obesity, and other disturbances in mice treated with monosodium glutamate. Science *164*, 719–721.

Olsson, M. (2011). PROPKA3: consistent treatment of internal and surface residues in empirical pKa predictions. J. Chem. Theory Comput. *7*, 525–537.

Pahk, A.J., and Williams, K. (1997). Influence of extracellular pH on inhibition by ifenprodil at N-methyl-D-aspartate receptors in Xenopus oocytes. Neurosci. Lett. *225*, 29–32.

Preskorn, S.H., Baker, B., Kolluri, S., Menniti, F.S., Krams, M., and Landen, J.W. (2008). An innovative design to establish proof of concept of the antidepressant effects of the NR2B subunit selective N-methyl-D-aspartate antagonist, CP-101,606, in patients with treatment-refractory major depressive disorder. J. Clin. Psychopharmacol. *28*, 631–637.

Ritschel, T., Hoertner, S., Heine, A., Diederich, F., and Klebe, G. (2009). Crystal structure analysis and in silico pKa calculations suggest strong pKa shifts of ligands as driving force for high-affinity binding to TGT. ChemBioChem *10*, 716–727.

Rowland, L.M. (2005). Subanesthetic ketamine: how it alters physiology and behavior in humans. Aviat. Space Environ. Med. *76* (*Suppl*), C52–C58.

Sacco, R.L., DeRosa, J.T., Haley, E.C., Jr., Levin, B., Ordronneau, P., Phillips, S.J., Rundek, T., Snipes, R.G., and Thompson, J.L.; Glycine Antagonist in Neuroprotection Americas Investigators (2001). Glycine antagonist in neuroprotection for patients with acute stroke: GAIN Americas: a randomized controlled trial. JAMA *285*, 1719–1728.

Saver, J.L. (2013). The 2012 Feinberg Lecture: treatment swift and treatment sure. Stroke *44*, 270–277.

Sherman, W., Day, T., Jacobson, M.P., Friesner, R.A., and Farid, R. (2006). Novel procedure for modeling ligand/receptor induced fit effects. J. Med. Chem. *49*, 534–553.

Shipman, S.T., Douglass, P.C., Yoo, H.S., Hinkle, C.E., Mierzejewski, E.L., and Pate, B.H. (2007). Vibrational dynamics of carboxylic acid dimers in gas and dilute solution. Phys. Chem. Chem. Phys. *9*, 4572–4586.

Smith, M.L., von Hanwehr, R., and Siesjö, B.K. (1986). Changes in extra- and intracellular pH in the brain during and following ischemia in hyperglycemic and in moderately hypoglycemic rats. J. Cereb. Blood Flow Metab. *6*, 574–583.

Sussman, F., Villaverde, M.C., Domínguez, J.L., and Danielson, U.H. (2013). On the active site protonation state in aspartic proteases: implications for drug design. Curr. Pharm. Des. *19*, 4257–4275.

Tahirovic, Y.A., Geballe, M., Gruszecka-Kowalik, E., Myers, S.J., Lyuboslavsky, P., Le, P., French, A., Irier, H., Choi, W.B., Easterling, K., et al. (2008). Enantiomeric propanolamines as selective N-methyl-D-aspartate 2B receptor antagonists. J. Med. Chem. *51*, 5506–5521.

Traynelis, S.F., Hartley, M., and Heinemann, S.F. (1995). Control of proton sensitivity of the NMDA receptor by RNA splicing and polyamines. Science *268*, 873–876.

Tzeli, D., Theodorakopoulos, G., Petsalakis, I.D., Ajami, D., and Rebek, J. (2011). Theoretical study of hydrogen bonding in homodimers and heterodimers of amide, boronic acid, and carboxylic acid, free and in encapsulation complexes. J. Am. Chem. Soc. *133*, 16977–16985.

Vance, K.M., Simorowski, N., Traynelis, S.F., and Furukawa, H. (2011). Ligand-specific deactivation time course of GluN1/GluN2D NMDA receptors. Nat. Commun. *2*, 294.

Vasileiou, C., Lee, K.S., Crist, R.M., Vaezeslami, S., Goins, S.M., Geiger, J.H., and Borhan, B. (2009). Dissection of the critical binding determinants of cellular retinoic acid binding protein II by mutagenesis and fluorescence binding assay. Proteins *76*, 281–290.

Wang, H., James, M.L., Venkatraman, T.N., Wilson, L.J., Lyuboslavsky, P., Myers, S.J., Lascola, C.D., and Laskowitz, D.T. (2014). pH-sensitive NMDA inhibitors improve outcome in a murine model of SAH. Neurocrit. Care *20*, 119–131.

Wood, P.L. (2005). The NMDA receptor complex: a long and winding road to therapeutics. IDrugs *8*, 229–235.

Wroge, C.M., Hogins, J., Eisenman, L., and Mennerick, S. (2012). Synaptic NMDA receptors mediate hypoxic excitotoxic death. J. Neurosci. *32*, 6732–6742.

Xiao, F., Pardue, S., Arnold, T., Carden, D., Alexander, J.S., Monroe, J., Sharp, C.D., Turnage, R., and Conrad, S. (2004). Effect of ifenprodil, a polyamine site NMDA receptor antagonist, on brain edema formation following asphyxial cardiac arrest in rats. Resuscitation *61*, 209–219.

Yang, Y., Li, Q., Yang, T., Hussain, M., and Shuaib, A. (2003). Reduced brain infarct volume and improved neurological outcome by inhibition of the NR2B subunit of NMDA receptors by using CP101,606-27 alone and in combination with rt-PA in a thromboembolic stroke model in rats. J. Neurosurg. *98*, 397–403.

Young, D. (2001). Computational Chemistry: A Practical Guide or Applying Techniques to Real World Problems. (New York: Wiley-Interscience), p. 330.

Yuan, H., Hansen, K.B., Vance, K.M., Ogden, K.K., and Traynelis, S.F. (2009). Control of NMDA receptor function by the NR2 subunit amino-terminal domain. J. Neurosci. *29*, 12045–12058.

Yurkewicz, L., Weaver, J., Bullock, M.R., and Marshall, L.F. (2005). The effect of the selective NMDA receptor antagonist traxoprodil in the treatment of traumatic brain injury. J. Neurotrauma *22*, 1428–1443.